

# Laser Powered Harvesting System for Table-Top Grown Strawberries

Mohamed Sorour, Pål Johan From

**Abstract**—In this paper, a novel tool prototype for harvesting table-top grown strawberries is presented. With robustness against strawberry localization error of  $\pm 15mm$  and average cycle time of 8.02 seconds at 50% of maximum operational velocity, it provides a promising contribution towards full automation of strawberry harvesting. In addition, the tool has an overall fruit-interacting width of 35mm that greatly enhances reach-ability due to the minimal footprint. A complete harvesting system is also proposed that can be readily mounted to a mobile platform for field tests. An experimental demonstration is performed to showcase the new methodology and derive relevant metrics.

**Index Terms**—fruit picking, strawberry harvesting, agriculture robotics.

## I. INTRODUCTION

On account of the seasonal nature of manual harvesting [1], [2], increasing demand for labours [3], [4] in competitive industrial sectors, as well as ageing farming society [5], the need for harvesting automation is well established and justified. Such unmet need, results in elevated cost of living [6] due to the higher costs incurred to secure labour, and lesser supply of crop, damaged for missing the optimal harvesting window. Harvesting robots developed so far, on the other hand, have an average success rate as low as 66% [7], subject to drastic drop in cluttered environment, mostly due to bulky harvesting tools [8].

Automated fruit harvesting essentially requires a tool that can: (1) capture the fruit, and (2) detach it. To capture, grasping is conventionally employed in the literature, harvesting apples [9]–[11], plums [12], kiwi [13], tomatoes [14], sweet pepper [15], [16], and strawberries [17]. Mechanical grasping mostly results in a bulky tool interacting with the produce, hindering as such reach-ability. Employing vacuum suction instead [18]–[22], reduces the tool size, but lead to complexity in finding the correct spot on the produce to apply, as well as being force-full. To detach, sharp mechanical cutter is by far the most commonly used method, enlarging the harvesting tool size, since the driving source (motor) and transmission must be very close to the cutting tool. Non-conventional cutting means are rare in the literature, featuring an oscillating blade to cut sweet pepper in [23], and a thermal cutting device in [24], [25] for cucumber and pepper respectively. Laser beam is used in [26], [27] to showcase the potential for cutting tomato peduncles, and in [28]–[31] for weed control. Despite the non-conventional cutting, bulky grasping is employed in the aforementioned research work.

In this work, the authors present a novel harvesting tool that virtually captures the fruit by surrounding it, and de-

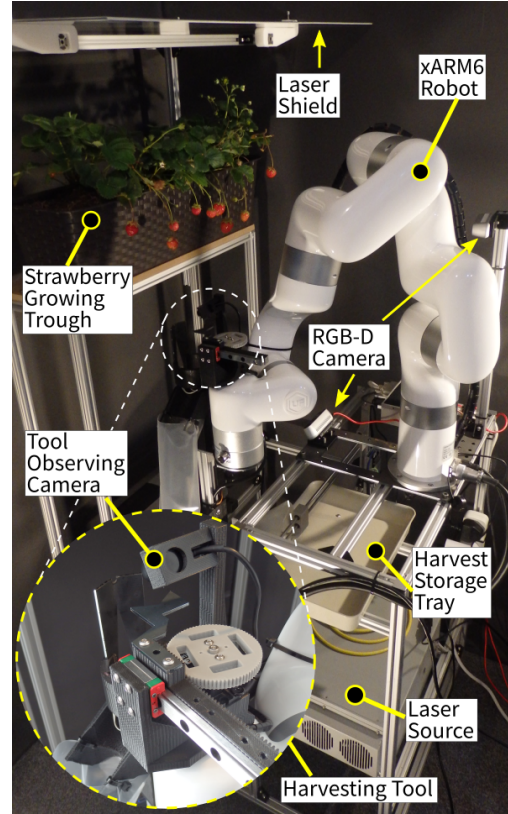


Fig. 1: Harvesting setup simulating an actual table-top strawberry growing system in poly-tunnels.

taches the stem by applying a highly focused laser beam from large distance, resulting in minimal interaction with the fruit and its local environment. In addition, the authors propose the harvesting system prototype shown in Fig. 1, with relative distances provided in Fig. 2 replicating those normally found in strawberry growing poly-tunnel setups. The system as such, can be readily mounted to a mobile robot for field harvesting, with minimal modifications required. The contribution of our approach is threefold:

- Productive: with average cycle time of 8 seconds at 50% of maximum robot velocity, in addition to the maintenance-free laser cutting.
- Small footprint: interacting hardware width of 35mm greatly enhances fruit reachability.
- Robust: precise stem entrapment tolerating strawberry localization error of up to  $\pm 15mm$ .

This paper is organised as follows, section II introduces the anatomy of the harvesting system and the operation logic. Algorithms for strawberry localization and harvesting as well as experiments are reported in section III. Conclusions are finally given in section IV.

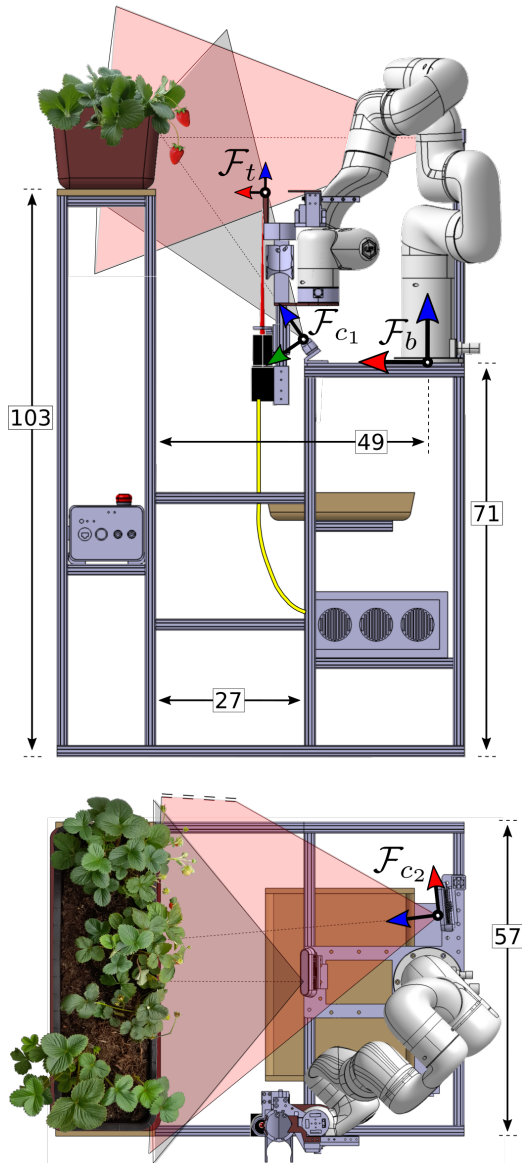


Fig. 2: The harvesting system anatomy in side and top views. Relevant coordinate frames are shown with x, y, and z axes in red, green and blue arrows respectively. Vision cone of first and second RGB-D cameras in grey and light red respectively. Selected dimensions of interest in centimeters.

## II. SYSTEM ANATOMY AND OPERATION LOGIC

The developed harvesting tool is shown in Fig. 3, two components interact with the strawberry namely; the stem trapping groove, and the stem trapper. Both are made of mild steel due to its low thermal conductivity (as compared to Aluminium for example), however, any ferrous metal will be as effective. When the laser beam is activated during the stem cutting process, this feature preserves the heat locally, helping the cutting process, killing plant viruses, and preventing the melt down of other plastic components of the tool. The width of both components is 35 and 30mm respectively, matching the dimensions of a large strawberry, as such, minimum fruit dislocation can be achieved during harvesting, as well as better fruit reach-ability. The opening between both parts acts as the strawberry entry side in [32], which

will approach the fruit from below, completely surround it, before performing the stem cut. A convex lens with focal length of 25cm focuses the fiber laser beam generated at the laser head below [33]. It is servo controlled to perform a lateral, reciprocating, straight line motion to drive the focal point into a line with controllable length to effectively cut the trapped strawberry-stem. Two infrared photo interrupters are used to detect the free falling strawberry after being detached, that is then led to a storage unit by means of a smooth plastic passage, protecting the fruit surface from damage.

The harvesting tool is mounted to a cost-effective 6 DOF collaborative robot arm system as shown in Fig. 2 in side and top views. A set of two RGB-D cameras mounted in different view points facing the strawberry growing trough, to the front and from below. The objective of such arrangement is to obtain a realistic point cloud of the scene with enough information to determine the location and the size of strawberries. The field of view of both cameras is depicted in the same figure, colored in light grey and red respectively, showing the common area of focus, at which strawberries can be mutually detected. This setup is based on an average table-top height of 103cm readily available at the poly-tunnel of the host institution, and the average Thorvald mobile robot height [34] widely used in field robotics. The robot arm base frame  $\mathcal{F}_b$  is related to the first  $\mathcal{F}_{c_1}$  and second  $\mathcal{F}_{c_2}$  camera frames by the constant transformation matrices  ${}^b\mathbf{T}_{c_1}$ , and  ${}^b\mathbf{T}_{c_2}$  respectively, and rigidly connected via the arm base plate. As such, the setup (arm, tool, and cameras) can be fitted to a mobile robot for field testing with minimal modification to the control algorithm. The tool tip frame  $\mathcal{F}_t$  is controlled to surround the fruit prior to harvesting, by manipulating the arm, it aligns with the tip of the stem trapping groove shown in Fig. 3. Let the

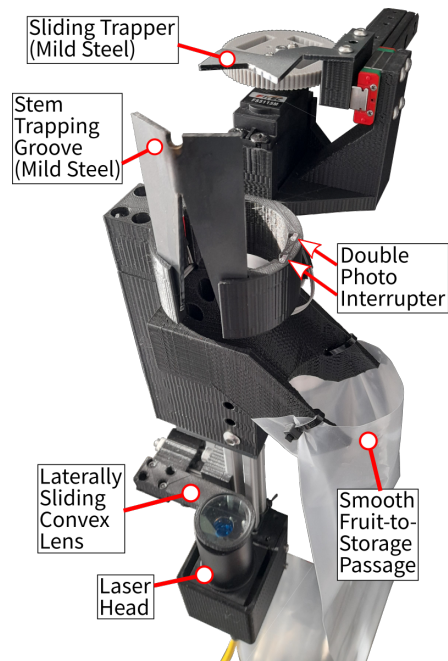


Fig. 3: The harvesting tool anatomy with the process observing camera omitted for convenience.

pose  ${}^b\mathbf{p}_t = [{}^b\mathbf{r}_t^\top {}^b\boldsymbol{\theta}_t^\top]^\top \in \mathbb{R}^6$  of the manipulator's tool tip frame  $\mathcal{F}_t$  expressed in the base frame  $\mathcal{F}_b$  define the task space coordinates. With  ${}^b\mathbf{r}_t = [x \ y \ z]^\top$  being the position vector, and  ${}^b\boldsymbol{\theta}_t = [\gamma \ \beta \ \alpha]^\top$  denoting a minimal representation of orientation (*roll, pitch, yaw* RPY variation of Euler angles). In this work, the tool tip frame orientation is fixed and identical to that of the base frame, as such, the tool pose  ${}^b\mathbf{p}_t$  notation will be dropped, and only the 3D tool position  ${}^b\mathbf{r}_t$  will be used in the sequel. The arm configuration shown in Fig. 2 corresponds to the HOME tool position  ${}^b\mathbf{r}_{\text{HOME}}$ , at which, the arm is not obstructing the field of vision of the cameras, and the strawberry localization algorithm (to be presented in the next section) can run.

The operation logic of the harvesting tool is depicted in Fig. 4. Following strawberry localization, the v-shaped stem-trapping-groove (note the sliding trapper is also v-shaped, but inverted) - refer to Fig. 4(c)(left) - is positioned immediately behind the berry-to-harvest at a lower z-axis position in Fig 4(a), the tool tip then elevates to isolate the fruit from its surrounding to the rear as shown in Fig. 4(b). The trapper then slides to trap the stem, with Fig. 4(c)(left) showing the first contact between both, and the eventually fully trapped stem in 4(c)(right). The laser beam is then activated to full power as in Fig. 4(d), and the convex lens reciprocates laterally with a stroke of  $6\text{mm}$  driving the focal point across the stem back and forth until the stem is cut. The mid-stroke is adjusted to the groove center point. Although the current tool design can force the stem into a precise location as compared to the author's previous work [32], a laser beam with large focal distance is still needed to minimize the volume of the hardware interacting with the fruit during the harvesting process. The trapper end of stroke is adjusted to minimize the stem relocation, and as such the strawberry, while maintaining a metallic background shield as the laser beam performs the cut, this is shown in the enlarged square in 4(d).

The tool, aims to approach the berry from below while perfectly aligned with the trapper groove. However, due to inaccuracies resulting from the point cloud calculation, and augmenting the depth information from two different sensors, localization errors can add up, this in addition to the naturally occurring stem bending. The width of the trapper of  $30\text{mm}$  ensures robustness against such errors within a tolerance of  $\pm 15\text{mm}$  from the actual strawberry location. This is shown in Fig. 4(b) and Fig. 4(c)(left), with imperfect strawberry localization. Fruit detachment is detected using two photo interrupters, the infrared beam of which is virtually shown in red color in Fig. 4(b) and 4(c) for clarification. Once any of the two beams is interrupted, the laser source is disengaged, terminating the cutting cycle, and the arm either moves to the next fruit to cut, or to the home position.

### III. CONTROL ALGORITHM AND EXPERIMENTS

In this section we present the algorithms for strawberry localization and motion control that are used in the harvesting experiment. In which, the system described in the previous section is used to harvest a collection of 9 strawberries in full autonomy, the point cloud of these depicted in Fig. 5. The hardware used feature the 6 DOF xARM6 collaborative

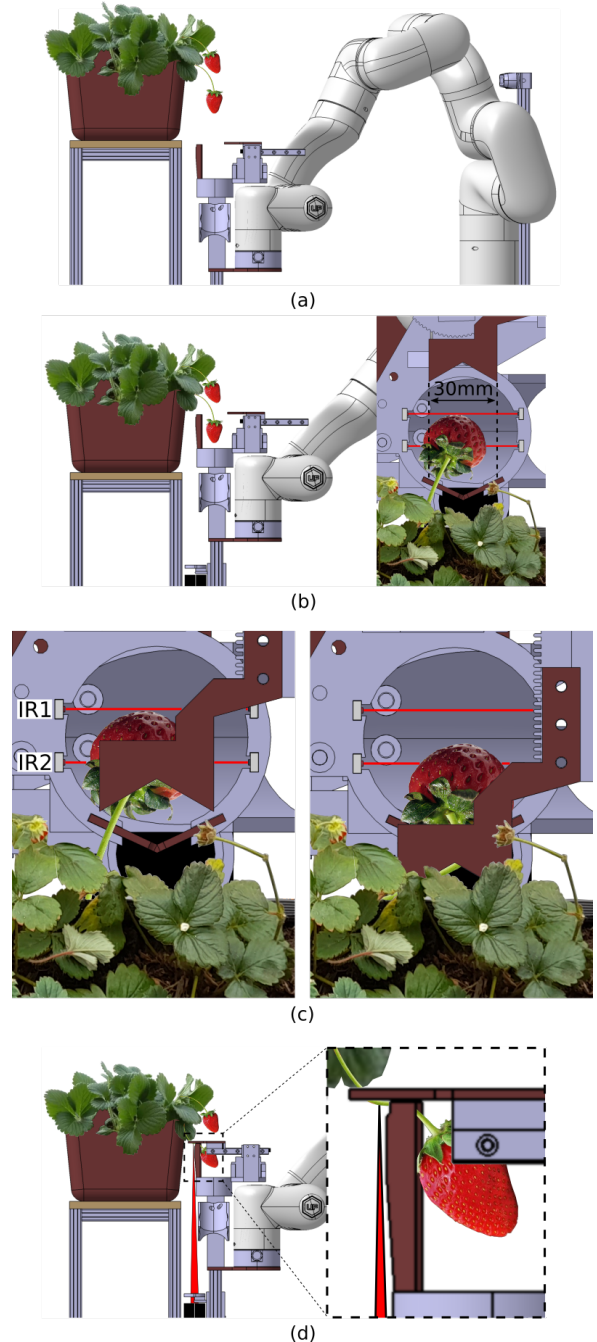


Fig. 4: Operation logic, with the harvesting tool at the x-y coordinates of the strawberry in (a), eventually encapsulating it by moving upwards in z-axis (b). The stem is precisely entrapment into a groove in (c) while tolerating fruit localization error, followed by triggering the laser beam in (d) until fruit detachment.

robot [35], two realsense D435 depth cameras, and a 50 Watts Raycus RFL-P50QB module [33] as the fiber laser source. The harvesting tool is 3D printed except for the stem-trapper and the trapping-groove that are subjected to extensive laser heat. Microcontroller is used to control the convex lens and trapper movements, the laser activation, as well as monitoring the strawberry detachment photo interrupters. On the software side, we use the realsense SDK library for interfacing with the cameras, and the Point Cloud

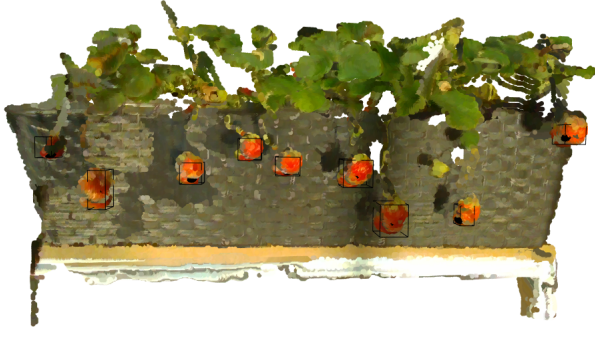


Fig. 5: Reduced scene point cloud focusing on the area of interest with black bounding box marking the located strawberries.

Library (PCL) [36]. A video of the harvesting experiment is submitted with this paper, also available on YouTube<sup>1</sup>, snapshots of which are shown in Fig. 6.

### A. Strawberry Localization

The pseudo-code for strawberry localization is provided in Algorithm 1, it takes as input the raw scene point cloud acquired by both RGB-D cameras  ${}^{c_1}\mathcal{C}_{s_1}$ , and  ${}^{c_2}\mathcal{C}_{s_2}$  expressed in the corresponding camera frame. These are then

---

#### Algorithm 1 Strawberry localization algorithm

---

**Input:** colored scene point cloud  ${}^{c_1}\mathcal{C}_{s_1}$  from RGB-D CAM1,  
colored scene point cloud  ${}^{c_2}\mathcal{C}_{s_2}$  from RGB-D CAM2.

**Output:** Vectors defining the bounding box for localized strawberries in arm base frame.

```

1:  ${}^b\mathcal{C}_s = {}^b\mathbf{T}_{c_1} {}^{c_1}\mathcal{C}_{s_1} + {}^b\mathbf{T}_{c_2} {}^{c_2}\mathcal{C}_{s_2}$ 
2:  ${}^b\mathcal{C}_{rs} = \emptyset$ 
3: for each point  ${}^b\mathbf{c}_s^i$  in  ${}^b\mathcal{C}_s$  do
4:   if ( ${}^b\mathbf{c}_s^i.x < x_l^+$  and  ${}^b\mathbf{c}_s^i.x > x_l^-$  and  ${}^b\mathbf{c}_s^i.y < y_l^+$  and
 ${}^b\mathbf{c}_s^i.y > y_l^-$  and  ${}^b\mathbf{c}_s^i.z < z_l^+$  and  ${}^b\mathbf{c}_s^i.z > z_l^-$ ) then
5:      ${}^b\mathcal{C}_{rs} \leftarrow {}^b\mathbf{c}_s^i$ 
6:   end if
7: end for
8:  ${}^b\mathcal{C}_{red} = \emptyset$ 
9: for each point  ${}^b\mathbf{c}_{rs}^i$  in  ${}^b\mathcal{C}_{rs}$  do
10:  if ( ${}^b\mathbf{c}_{rs}^i.r > r_{th}$  and  ${}^b\mathbf{c}_{rs}^i.g < g_{th}$  and  ${}^b\mathbf{c}_{rs}^i.b < b_{th}$ ) then
11:     ${}^b\mathcal{C}_{red} \leftarrow {}^b\mathbf{c}_{rs}^i$ 
12:  end if
13: end for
14:  ${}^b\mathcal{C}_{straw} = \text{EuCS}(t, s_{min}, s_{max}, {}^b\mathcal{C}_{red})$ 
15: for each cluster  ${}^b\mathbf{c}_{straw}^i$  in  ${}^b\mathcal{C}_{straw}$  do
16:   ${}^b\mathbf{x}_{straw}^{min} \leftarrow \text{MIN}({}^b\mathbf{c}_{straw}^i, 0)$ 
17:   ${}^b\mathbf{x}_{straw}^{max} \leftarrow \text{MAX}({}^b\mathbf{c}_{straw}^i, 0)$ 
18:   ${}^b\mathbf{y}_{straw}^{min} \leftarrow \text{MIN}({}^b\mathbf{c}_{straw}^i, 1)$ 
19:   ${}^b\mathbf{y}_{straw}^{max} \leftarrow \text{MAX}({}^b\mathbf{c}_{straw}^i, 1)$ 
20:   ${}^b\mathbf{z}_{straw}^{min} \leftarrow \text{MIN}({}^b\mathbf{c}_{straw}^i, 2)$ 
21:   ${}^b\mathbf{z}_{straw}^{max} \leftarrow \text{MAX}({}^b\mathbf{c}_{straw}^i, 2)$ 
22: end for
23: return  ${}^b\mathbf{x}_{straw}^{min}, {}^b\mathbf{x}_{straw}^{max}, {}^b\mathbf{y}_{straw}^{min}, {}^b\mathbf{y}_{straw}^{max},$ 
 ${}^b\mathbf{z}_{straw}^{min}, {}^b\mathbf{z}_{straw}^{max}$ 

```

---

<sup>1</sup>[https://youtu.be/W3UyDt\\_7erA](https://youtu.be/W3UyDt_7erA).

transformed to the arm base frame and augmented (code line 1) to form the scene point cloud  ${}^b\mathcal{C}_s$ . From which, a *reduced scene* cloud set  ${}^b\mathcal{C}_{rs} \subset {}^b\mathcal{C}_s$  is then constructed, where a point  ${}^b\mathbf{c}_s^i$  in the scene cloud  ${}^b\mathcal{C}_s$  is added to the reduced cloud if it resides in a spatial window characterized by the maximum and minimum limits  $x_l^+, x_l^-, y_l^+, y_l^-, z_l^+, z_l^-$  in  $x, y$ , and  $z$  coordinates respectively of the arm base frame. This reduces the forthcoming computation to the area of interest that is dexterously accessible by the robot arm, such reduced point cloud is shown in Fig. 5. Ripe strawberries are simply extracted by thresholding the red color using the RGB thresholds  $r_{th}, g_{th}, b_{th}$  to form the *red* point cloud  ${}^b\mathcal{C}_{red} \subset {}^b\mathcal{C}_{rs}$ . We then use the PCL implemented Euclidean cluster segmentation algorithm to segment each individual strawberry. The output of the function  $\text{EuCS}(t, s_{min}, s_{max}, {}^b\mathcal{C}_{red})$  is a set of strawberry clusters (set of point clouds each representing a single strawberry)  ${}^b\mathcal{C}_{straw}$  arranged in ascending order of the y-axis coordinate values. With  $t, s_{min}, s_{max}$  denoting the segmentation tolerance, minimum and maximum cluster sizes respectively. The  $\text{MIN}({}^b\mathbf{c}_{straw}^i, 0)$  function, supplied with a point cloud  ${}^b\mathbf{c}_{straw}^i$  and an index, will return the minimum value available at such index in all point cloud points, whereas, supplied with a vector, will return the smallest value irrespective of the index. The lengthy pseudo-code for the aforementioned two functions is omitted for convenience. Values of the parameters used in Algorithm 1 is provided in Table I. The output is a set of vectors defining the bounding boxes of the localized strawberries, these boxes are shown in Fig. 5.

### B. Harvesting Motion

Pseudo-code of the harvesting algorithm is provided in Algorithm 2, it is also depicted in Fig. 6. It takes as input, the vectors defining the bounding box of the identified/localized strawberries, that is the output of the localization algorithm in Algorithm 1. The output is a series of commands to control the robot arm movement, as well as controlling the stem-trapper and the laser module. In this work, a strawberry cutting cycle, and as such the cycle time, starts and ends with a single strawberry unit being detached. Initially, the algorithm moves the robot arm to the home position  $\mathbf{r}_{\text{HOME}}$  (configuration depicted in Fig. 2), the  $\text{ROBOT\_MOVE}()$  function in Algorithm 2 is blocking (has to be finished before executing the next line of code). It then computes a minimal z-axis point  ${}^b z_{min}$ , corresponding to the lowest hanging strawberry observed. In Fig. 6(a), a strawberry unit has just been cut, signaling the start of a new cycle, at which the robot arm moves to  ${}^b z_{min}$ , as shown in Fig. 6(b) consuming 1.77 seconds. By setting  ${}^b\mathbf{r}_t^d(2) = {}^b z_{min}$ , only the z-axis component of the desired tool position vector  ${}^b\mathbf{r}_t^d$  is changed,

TABLE I: Localization algorithm parameters

Parameter	Value(unit)	Parameter	Value(unit)
$x_l^+$	55(cm)	$r_{th}$	100
$x_l^-$	25(cm)	$g_{th}$	70
$y_l^+$	30(cm)	$b_{th}$	70
$y_l^-$	-30(cm)	$t$	0.02(cm)
$z_l^+$	50(cm)	$s_{min}$	20
$z_l^-$	30(cm)	$s_{max}$	1000

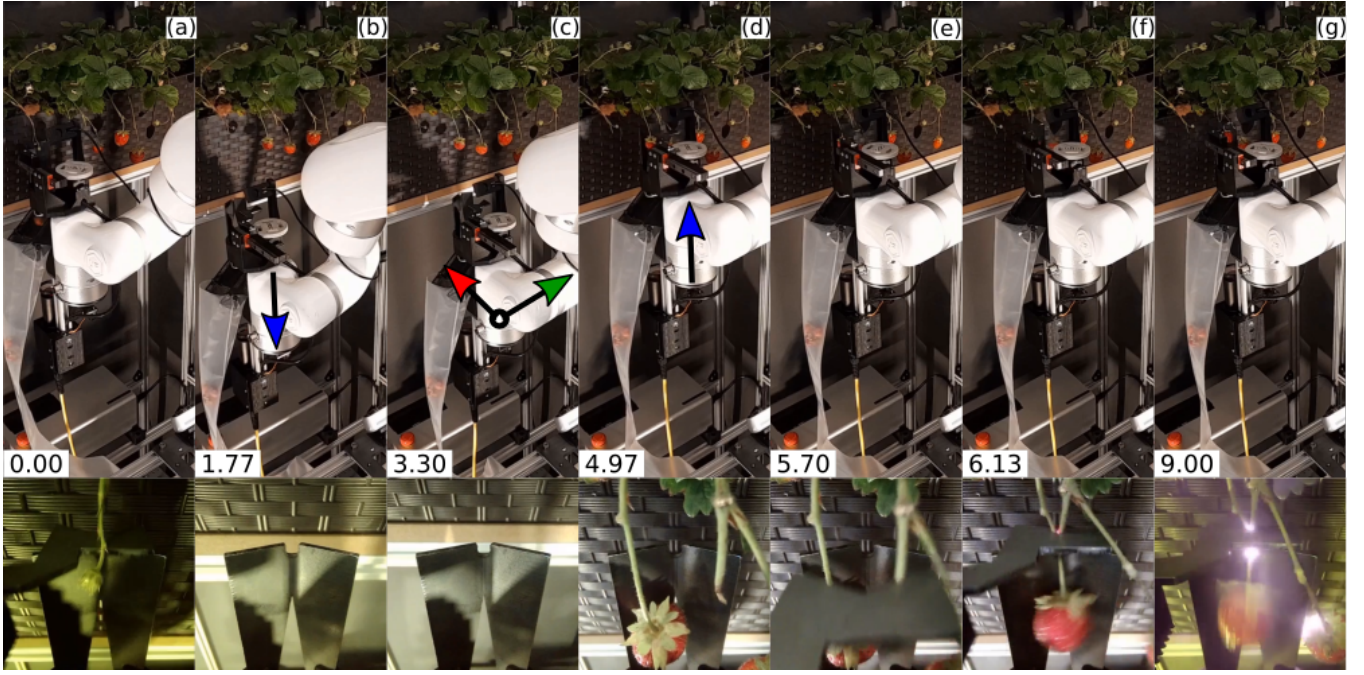


Fig. 6: Snapshots of a complete strawberry harvesting cycle, starting and ending with the detachment of a single strawberry, indicating the time stamp (in seconds) of each step in-between. Lower row showing the close-up images captured by the tool-observing camera.

while retaining the old values for the other two components (x and y axes). The arm then moves to the x-y coordinates of the next detected strawberry using the information of the corresponding bounding box, before moving upwards in z-axis as shown in Fig. 6(c) and Fig. 6(d) respectively. In order to compensate for the probable inaccuracy in measuring the actual depth of strawberry, an empirically determined safety factor is added to the maximum boundary computed in x and z axes (code lines 6 and 9 in Algorithm 2). To this end, the robot arm motion for this cycle is finished, what remains is

---

#### Algorithm 2 Harvesting algorithm

---

**Input:**  $b_{x_{straw}}^{max}$ ,  $b_{y_{straw}}^{min}$ ,  $b_{y_{straw}}^{max}$ ,  $b_{z_{straw}}^{min}$ ,  $b_{z_{straw}}^{max}$   
**Output:** desired tool tip position in arm base frame  $b_{\mathbf{r}_t^d}$ .

- 1: ROBOT\_MOVE ( $b_{\mathbf{r}_{HOME}}$ )
- 2:  $b_{z_{min}} = \text{MIN}(b_{z_{straw}}^{min}) - 10\text{mm}$
- 3: **for each** strawberry unit  $i$  in  $n_{straw}$  **do**
- 4:    $b_{\mathbf{r}_t^d}(2) = b_{z_{min}}$
- 5:   ROBOT\_MOVE ( $b_{\mathbf{r}_t^d}$ )
- 6:    $b_{\mathbf{r}_t^d}(0) = b_{x_{straw}}^{max}(i) + 10\text{mm}$
- 7:    $b_{\mathbf{r}_t^d}(1) = (b_{y_{straw}}^{min}(i) + b_{y_{straw}}^{max}(i))/2$
- 8:   ROBOT\_MOVE ( $b_{\mathbf{r}_t^d}$ )
- 9:    $b_{\mathbf{r}_t^d}(2) = b_{z_{straw}}^{max}(i) + 15\text{mm}$
- 10:   ROBOT\_MOVE ( $b_{\mathbf{r}_t^d}$ )
- 11:   TRAP\_STEM()
- 12:   **while** IR1 **and** IR2 **do**
- 13:     LASER(ON)
- 14:   **end while**
- 15:   LASER(OFF)
- 16:   RELEASE\_STEM()
- 17: **end for**
- 18: ROBOT\_MOVE ( $b_{\mathbf{r}_{HOME}}$ )

---

the cutting procedure, that is microcontroller implemented. When given the signal to perform the cut, the microcontroller actuates the trapper forward using TRAP\_STEM(), then activates the laser module as well as the convex lens lateral movement using LASER(ON) until any of the photo interrupters IR1 or IR2 (refer to Fig. 4) detects the detached fruit. At which instance, the laser beam is deactivated and the trapper moves backwards.

The average cycle and stem-cut time is 8.02, and 2.3 seconds respectively, with the robot arm operating at 50% of maximum velocity for hardware safety reasons. The localization algorithm consumes 100ms in worst case scenario on a standard laptop with intel core-i7 processor. The maintenance-free laser cutting has a long term positive impact on productivity, as compared to literature-dominating mechanical cutting tools that require frequent replacement. To this end, the authors believe that a 3D linear system replacing the robot arm, in addition to a 100 Watt laser module (following the conclusions in [37]) can reduce the average cycle time below the 4 seconds mark, cutting the gap with the average manual picking cycle standing at 1.5s [38]. That, in addition to further enhancing the fruit identification and localization algorithm, would greatly update the current development status [39] thanks to the minimal footprint of the developed tool.

#### IV. CONCLUSION

In this work, a novel harvesting prototype has been presented, customised for table-top grown strawberries. It employs a trapping mechanism to surround the fruit and force the stem into a pre-defined position where a focused laser beam performs the cut. The proposed harvesting tool is robust against localization errors while maintaining small

footprint for enhancing fruit reachability. Successful harvest-demonstration confirm the effectiveness of the novel methodology.

## REFERENCES

- [1] K. Nolte and M. Ostermeier, "Labour market effects of large-scale agricultural investment: Conceptual considerations and estimated employment effects," *World Development*, vol. 98, pp. 430–446, 2017.
- [2] U. Government, "The impact on the horticulture and food processing sectors of closing the seasonal agricultural workers scheme and the sectors based scheme," [https://assets.publishing.service.gov.uk/government/uploads/system/uploads/attachment\\_data/file/257242/migrant-seasonal-workers.pdf](https://assets.publishing.service.gov.uk/government/uploads/system/uploads/attachment_data/file/257242/migrant-seasonal-workers.pdf), last accessed 18/02/2022, May 2013.
- [3] T. W. Bank, "Employment in agriculture (percentage of total employment) (modeled ilo estimate)," <https://data.worldbank.org/indicator/SL.AGR.EMPL.ZS>, accessed 12/06/2021.
- [4] N. F. U. UK, "Establishing the labour availability issues of the uk food and drink sector," <https://www.nfonline.com/archive?treeid=152097>, last accessed 18/02/2022, August 2021.
- [5] T. Duckett, S. Pearson, S. Blackmore, and B. Grieve, "Agricultural robotics: The future of robotic agriculture," *EPSRC UK Robotics and Autonomous Systems (RAS) Network*, 2018. [Online]. Available: <http://arxiv.org/abs/1806.06762>
- [6] A. Cassey, K. Lee, J. Sage, and P. Tozer, "Assessing post-harvest labor shortages, wages, and welfare," *Agricultural and Food Economics*, vol. 6, 2018.
- [7] C. W. Bac, E. J. van Henten, J. Hemming, and Y. Edan, "Harvesting robots for high-value crops: State-of-the-art review and challenges ahead," *Journal of Field Robotics*, vol. 31, no. 6, pp. 888–911, 2014.
- [8] G. Kootstra, X. Wang, P. M. Blok, J. Hemming, and E. van Henten, "Selective harvesting robotics: Current research, trends, and future directions," *Current Robotics Reports*, vol. 2, pp. 95–104, 2021.
- [9] Z. De-An, L. Jidong, J. Wei, Z. Ying, and C. Yu, "Design and control of an apple harvesting robot," *Biosystems Engineering*, vol. 110, no. 2, pp. 112–122, 2011. [Online]. Available: <https://www.sciencedirect.com/science/article/pii/S1537511011001206>
- [10] A. Silwal, J. R. Davidson, M. Karkee, C. Mo, Q. Zhang, and K. Lewis, "Design, integration, and field evaluation of a robotic apple harvester," *Journal of Field Robotics*, vol. 34, no. 6, pp. 1140–1159, 2017. [Online]. Available: <https://onlinelibrary.wiley.com/doi/abs/10.1002/rob.21715>
- [11] Y. Onishi, T. Yoshida, H. Kurita, T. Fukao, H. Arihara, and A. Iwai, "An automated fruit harvesting robot by using deep learning," *ROBOMECH Journal*, vol. 6, 2019.
- [12] J. Brown and S. Sukkarieh, "Design and evaluation of a modular robotic plum harvesting system utilizing soft components," *Journal of Field Robotics*, vol. 38, no. 2, pp. 289–306, 2021.
- [13] L. Mu, G. Cui, Y. Liu, Y. Cui, L. Fu, and Y. Gejima, "Design and simulation of an integrated end-effector for picking kiwifruit by robot," *Information Processing in Agriculture*, vol. 7, no. 1, pp. 58–71, 2020. [Online]. Available: <https://www.sciencedirect.com/science/article/pii/S2214317318304372>
- [14] Q. Feng, X. Wang, G. Wang, and Z. Li, "Design and test of tomatoes harvesting robot," in *2015 IEEE International Conference on Information and Automation*, 2015, pp. 949–952.
- [15] B. Arad, J. Balendonck, R. Barth, O. Ben-Shahar, Y. Edan, T. Hellström, J. Hemming, P. Kurtser, O. Ringdahl, T. Tielen, and B. van Tuijl, "Development of a sweet pepper harvesting robot," *Journal of Field Robotics*, vol. 37, no. 6, pp. 1027–1039, 2020.
- [16] C. W. Bac, J. Hemming, B. van Tuijl, R. Barth, E. Wais, and E. J. van Henten, "Performance evaluation of a harvesting robot for sweet pepper," *Journal of Field Robotics*, vol. 34, no. 6, pp. 1123–1139, 2017.
- [17] Y. Xiong, C. Peng, L. Grimstad, P. J. From, and V. Isler, "Development and field evaluation of a strawberry harvesting robot with a cable-driven gripper," *Computers and Electronics in Agriculture*, vol. 157, pp. 392–402, 2019. [Online]. Available: <https://www.sciencedirect.com/science/article/pii/S0168169918312456>
- [18] J. Baeten, K. Donné, S. Boedrij, W. Beckers, and E. Claesen, *Autonomous Fruit Picking Machine: A Robotic Apple Harvester*. Berlin, Heidelberg: Springer Berlin Heidelberg, 2008, pp. 531–539.
- [19] K. Tanigaki, T. Fujiura, A. Akase, and J. Imagawa, "Cherry-harvesting robot," *Computers and Electronics in Agriculture*, vol. 63, no. 1, pp. 65–72, 2008, special issue on bio-robotics. [Online]. Available: <https://www.sciencedirect.com/science/article/pii/S0168169908000458>
- [20] S. Hayashi, K. Shigematsu, S. Yamamoto, K. Kobayashi, Y. Kohnno, J. Kamata, and M. Kurita, "Evaluation of a strawberry-harvesting robot in a field test," *Biosystems Engineering*, vol. 105, no. 2, pp. 160–171, 2010. [Online]. Available: <https://www.sciencedirect.com/science/article/pii/S1537511009002797>
- [21] S. Hayashi, S. Yamamoto, S. Tsubota, Y. Ochiai, K. Kobayashi, J. Kamata, M. Kurita, H. Inazumi, and R. Peter, "Automation technologies for strawberry harvesting and packing operations in japan 1," *Journal of Berry Research*, vol. 4, 2014.
- [22] G. Hu, C. Chen, J. Chen, L. Sun, A. Sugirbay, Y. Chen, H. Jin, S. Zhang, and L. Bu, "Simplified 4-dof manipulator for rapid robotic apple harvesting," *Computers and Electronics in Agriculture*, vol. 199, p. 107177, 2022.
- [23] C. Lehnert, A. English, C. McCool, A. W. Tow, and T. Perez, "Autonomous sweet pepper harvesting for protected cropping systems," *IEEE Robotics and Automation Letters*, vol. 2, no. 2, pp. 872–879, 2017.
- [24] E. van Henten, J. Hemming, B. van Tuijl, B. van Tuijl, J. Kornet, J. Meuleman, J. Bontsema, and E. van Os, "An autonomous robot for harvesting cucumbers in greenhouses," *Autonomous Robots*, vol. 13, no. 3, pp. 241–258, 2002.
- [25] S. BACHCHE and K. OKA, "Performance testing of thermal cutting systems for sweet pepper harvesting robot in greenhouse horticulture," *Journal of System Design and Dynamics*, vol. 7, no. 1, pp. 36–51, 2013.
- [26] J. Liu, Z. Li, P. Li, and H. Mao, "Design of a laser stem-cutting device for harvesting robot," in *2008 IEEE International Conference on Automation and Logistics*, 2008, pp. 2370–2374.
- [27] J. Liu, Y. Hu, X. Xu, and P. Li, "Feasibility and influencing factors of laser cutting of tomato peduncles for robotic harvesting," *African Journal of Biotechnology*, vol. 10, no. 69, pp. 15552–15563, 2011.
- [28] T. Heisel, J. Schou, C. Andreasen, and S. Christensen, "Using laser to measure stem thickness and cut weed stems," *Weed Research*, vol. 42, no. 3, pp. 242–248, 2002. [Online]. Available: <https://onlinelibrary.wiley.com/doi/abs/10.1046/j.1365-3180.2002.00282.x>
- [29] S. K. Mathiassen, T. Bak, S. Christensen, and P. Kudsk, "The effect of laser treatment as a weed control method," *Biosystems Engineering*, vol. 95, no. 4, pp. 497–505, 2006. [Online]. Available: <https://www.sciencedirect.com/science/article/pii/S1537511006002984>
- [30] G. Coleman, C. Betters, C. Squires, S. Leon-Saval, and M. Walsh, "Low energy laser treatments control annual ryegrass (*Lolium rigidum*)," *Frontiers in Agronomy*, vol. 2, p. 35, 2021. [Online]. Available: <https://www.frontiersin.org/article/10.3389/fagro.2020.601542>
- [31] M. Nadimi, D. Sun, and J. Paliwal, "Recent applications of novel laser techniques for enhancing agricultural production," *Laser Physics*, vol. 31, no. 5, 2021.
- [32] M. Sorour, P. J. From, K. Elgeneidy, S. Kanarachos, and M. Sallam, "Produce harvesting by laser stem-cutting," in *2022 IEEE International Conference on Automation Science and Engineering*, 2022, p. to be published.
- [33] Raycus, "50w q-switched pulse fiber laser," <https://en.raycuslaser.com/products/50w-q-switched-pulse-fiber-laser.html>, last accessed 05/09/2022, 2022.
- [34] L. Grimstad and P. J. From, "Thorvald ii - a modular and re-configurable agricultural robot," *IFAC-PapersOnLine*, vol. 50, no. 1, pp. 4588–4593, 2017, 20th IFAC World Congress. [Online]. Available: <https://www.sciencedirect.com/science/article/pii/S2405896317314830>
- [35] xARM, "xarm collaborative robot," <https://www.ufactory.cc/xarm-collaborative-robot>, last accessed 05/09/2022, 2022.
- [36] R. B. Rusu and S. Cousins, "3D is here: Point Cloud Library (PCL)," in *IEEE International Conference on Robotics and Automation (ICRA)*, Shanghai, China, May 9–13 2011.
- [37] M. Sorour, P. J. From, K. Elgeneidy, S. Kanarachos, and M. Sallam, "Compact strawberry harvesting tube employing laser cutter," in *2022 IEEE/RSJ International Conference on Intelligent Robots and Systems (IROS)*, 2022, pp. 8956–8962.
- [38] S. Woo, D. D. Uyeh, J. Kim, Y. Kim, S. Kang, K. C. Kim, S. Y. Lee, Y. Ha, and W. S. Lee, "Analyses of work efficiency of a strawberry-harvesting robot in an automated greenhouse," *Agronomy*, vol. 10, no. 11, 2020.
- [39] H. Zhou, X. Wang, W. Au, H. Kang, and C. Chen, "Intelligent robots for fruit harvesting: recent developments and future challenges," *Precision Agriculture*, pp. 1573–1618, 2022.